Batteries & Supercaps

Research Article
doi.org/10.1002/batt.202300056

Chemistry Europe
European Chemical Societies Publishing

www.batteries-supercaps.org

VIP *Very Important Paper*

A Flexible Solid Polymer Electrolyte based Polymerized Ionic Liquid for High Performance Solid-State Batteries

Yuxiang Liu,[a] Furui Ma,*[a] Wenpeng Li,*[a] Ligang Gai,[a] Haohua Yang,[a] and Zengqi Zhang[b]

Solid polymer electrolytes (SPEs) combine the benefits of ceramic electrolyte and polymer electrolyte, and have broad application prospects in high-energy lithium metal batteries. However, low Li^+ conductivity and tensile strength are crucial elements that hinder the application of solid polymer electrolytes. In this paper, an effective solid polymer electrolyte was proposed to solve these problems. A polymerized ionic liquid (PIL) was chosen as the ionic transport material to synthesize three-dimensional cross-linked ion channels through thermal polymerization, which can effectively improve the ionic conductivity. This work is different from some other reports that add ionic liquid without C=C double bond. We used the vinyl ionic liquid (IL) as matrix via polymerization with azobis initiator (AIBN) and the obtained co-polymer has excellent flexibility and non-flowing character. $Li_{6.4}La_3Zr_{1.4}Ta_{0.6}O_{12}$ (LLZTO) ceramic filler was added to enhance the thermal stability and tensile strength of the electrolyte. Meanwhile, solid-state batteries (SSBs) assembled with $LiFePO_4$ cathode and high-voltage $LiNi_{0.8}Co_{0.1}Mn_{0.1}O_2$ cathode can deliver remarkable cell performance. This work presents an appropriate device for the structure of modern polymerized ionic liquid solid polymer electrolytes, and shows significant implication for the progress of high-property polymer electrolytes.

Introduction

With the development of the new energy industry, it is a general trend to explore a new generation of efficient energy storage equipment. The advantages of lithium-ion batteries (LIBs) are mainly due to the super-high theoretical capacity (3860 mA h g^{-1}) and the low redox potential (−3.04 V vs. SHE) of lithium metal. The LIBs have been expected to be the important part of electrochemical energy storage.[1–6] Nevertheless, the liquid electrolytes have safety issues such as the short circuit and explosion derived from the dendrite growth, attract the hazardous accidents and restrain the progress of LIBs.[7] Solid-state electrolytes (SSEs), such as solid polymer electrolytes (SPEs) and inorganic ceramic electrolytes (ICEs), containing no volatile and flammable organic plasticizers, can basically solve the security problems and enhance the energy density of LIBs. Therefore, it has steadily become a research focus.[8,9]

SPEs exhibit a series of virtues such as high stability, flexibility, approachable scalability, and intimate contact. They are identified as the next-generation flexible electrolyte candidate for SSBs.[10–12] Despite they have wide application prospects, SPEs are currently faced with certain main issues: 1) the unsatisfactory Li^+ conductivity at room temperature and the comparatively low lithium-ion transference number (t_{Li+}); 2) slow interface transport of Li^+ ions on account of the bad interface compatibility; 3) interface instability during extended battery cycling.[13,14] Up to now, some methods have been designed to settle the above issues, such as introduce inorganic fillers and liquid plasticizers, which can significantly improve ionic conductivity and considerably enhance t_{Li+}.[15–18] The incorporation of ionic liquids as plasticizers was considered as a potential method to enhance the interface compatibility and ionic conductivity of the SPEs.[19,20] But, in terms of the safety performance and the progress of the electrochemistry field, all-solid-state batteries without plasticizers are still the current hotspot.

Inspired by the above problems, we synthesized a kind of solid polymer electrolyte with ion channel network. Polymerized ionic liquid (PIL) was utilized in the polymer matrix, which can effectively enhance the Li^+ conductivity and Li^+ transference number. There were some indispensable superiorities of the IL ($VBImNTF_2$) was chosen for the polymer matrix as follows: (1) the low flammability and favorable thermal stability effectually alleviates the hazard of short circuit and combustion; (2) the high Li^+ conductivity and low volatility; (3) append IL could supply excess $TFSI^-$ with the concern of solvable $TFSI^-$, which is conductive to construct a stable heterogeneous artificial SEI layer.[21,22] In addition, PVDF-HFP is added to enhance the film-forming property of dielectrics, as a co-polymer, which has good film-forming property. The vinylidene fluoride (VDF) units play a vital role in forming the independent standing film, whereas the hexafluoropropylene (HFP) units can promote ion transport.[23,24]

Herein, we prepared a novel SPEs based on polymerized ionic liquid. The novel SPEs can form continuous intercon-

[a] *Y. Liu, Dr. F. Ma, Prof. W. Li, Prof. L. Gai, H. Yang*
Engineering & Technology Center of Electrochemistry, School of Chemistry and Chemical Engineering, Qilu University of Technology (Shandong Academy of Sciences)
250353 Jinan, China
E-mail: mafr@qlu.edu.cn
wenpengli75@163.com
[b] *Dr. Z. Zhang*
Qingdao Institute of Bioenergy and Bioprocess Technology, Chinese Academy of Sciences
266101 Qingdao, China

Supporting information for this article is available on the WWW under https://doi.org/10.1002/batt.202300056

Research Article
doi.org/10.1002/batt.202300056
Chemistry Europe
European Chemical Societies Publishing

nected ion migration channels, which can accelerate the polymer chains dynamics effectually, decrease crystallinity, and enhance ion conductivity of electrolytes. For purpose of enhancing the mechanical and electrochemical properties of polymer electrolyte, diverse contents of LLZTO were added into polymer electrolyte, and then the properties of ion conductivity, ion transfer number and electrochemical stability window were studied. After a certain amount of LLZTO added, the Li^+ conductivity of IPL21-SPE was up to 9.26×10^{-4} S cm^{-1} at 25 °C. The improved Li^+ conductivity can be mainly ascribed to the reduced crystallinity and the combined action between LLZTO particles and LiTFSI, which expedite the dissociation of LiTFSI. Moreover, because of LLZTO can decrease the crystallinity of PVDF-HFP, further promote the Li^+ conductivity, as well as improve the interface performance of electrode/electrolyte. In addition, the electrochemical stability window and ion transfer number are significantly improved, which are conducive to the assembly of all-solid-state batteries. The simple and efficient design points out the direction for the progress of solid polymer electrolytes with excellent Li^+ conductivity and satisfactory tensile properties.

Results and Discussion

The solid polymer electrolyte films were prepared by the solution casting method. The flow diagram was put forward in Figure 1. PIL and other components were uniformly dispersed in the solid electrolyte to form an unobstructed Li^+ transport pathway, which was beneficial to realize high Li^+ conductivity and enhance Li^+ mobility, as illustrated in Figure 2(a). It was worth noting that the prepared pure PVDF-HFP SPE membrane was uneven and had many folds. The top-view SEM images of IPL21-SPE in Figures 2(b) and S1 show that the microstructure of IPL21-SPE membrane was more uniform and flexibility, indicating the well dispersity of LLZTO powder in the electrolyte film. LLZTO can adjust the Li^+ movement in the three-dimensional ion channels, thereby realizing homogeneous Li^+ distribution and no lithium dendrite.[25] The films had excellent flexibility and did not fracture even after multiple folding and coiling (Figures 2b and S2), indicating that the superior tensile property can meet experimental condition.

The excellent mechanical properties of SPE are the key to flexible LIBs. The strains and stresses of composite polymers with different proportions were characterized and summarized. With the addition of PIL, the tensile strength gradually decreases, and the breaking elongation increases initially and then decreases (Figure S3b). The addition of ionic liquid polymers facilitates the conversion process of the polymer network structure from sparse to dense, and the increased number of the join points betwixt polymer chains restrains the motion of molecular chains. By comparing diverse electrolyte in the experiment, it can be seen that σ (IP21-SPE) $>\sigma$ (IP31-SPE) $>\sigma$ (IP11-SPE). According to the formula, the Li^+ conductivity of IP21-SPE is 2.76×10^{-4} S cm^{-1} at 25 °C. When the temperature rises to 70 °C, the conductivity increases to 2.11×10^{-3} S cm^{-1}. A certain linear dependence of IP21-SPE electrolyte between the Li^+ conductivity and the test temperature, was coincident with the fitting curve (Figure S3a). IP21-SPE was selected as the further research object under comprehensive consideration of the mechanical strength and Li^+ conductivity.

As displayed in Figure 2(c), the inhibitory effect of polymer crosslinking network on PVDF-HFP crystallization was verified by XRD spectra. Generally, on account of the Li^+ migration mainly existing in the amorphous area, the Li^+ conductivity can be improved by decreasing the crystallinity of polymer electrolyte. Compared with pure PH-SPE, the diffraction peak shape of IP21-SPE is smoother, reflecting that the polymerization of ionic

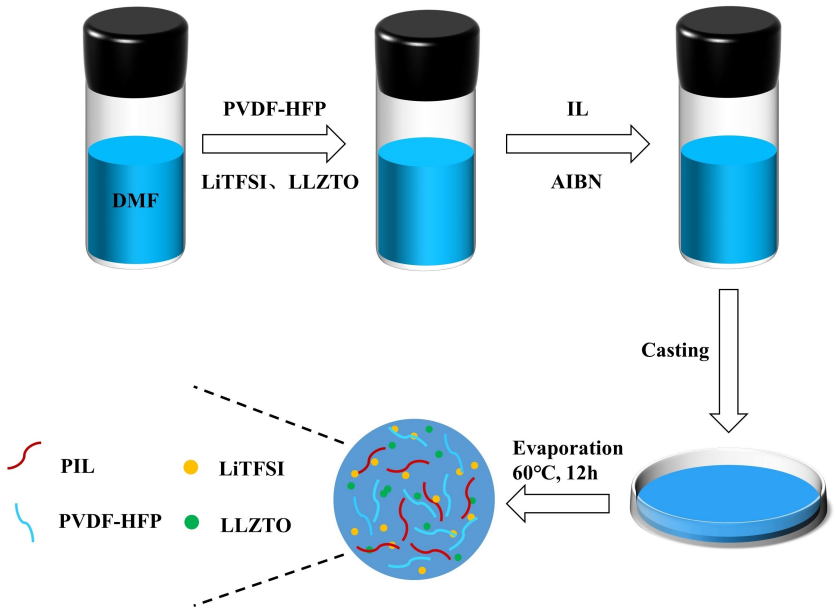

Figure 1. Schematic diagram of the SPE films preparation process.

Research Article
doi.org/10.1002/batt.202300056
Chemistry Europe
European Chemical Societies Publishing

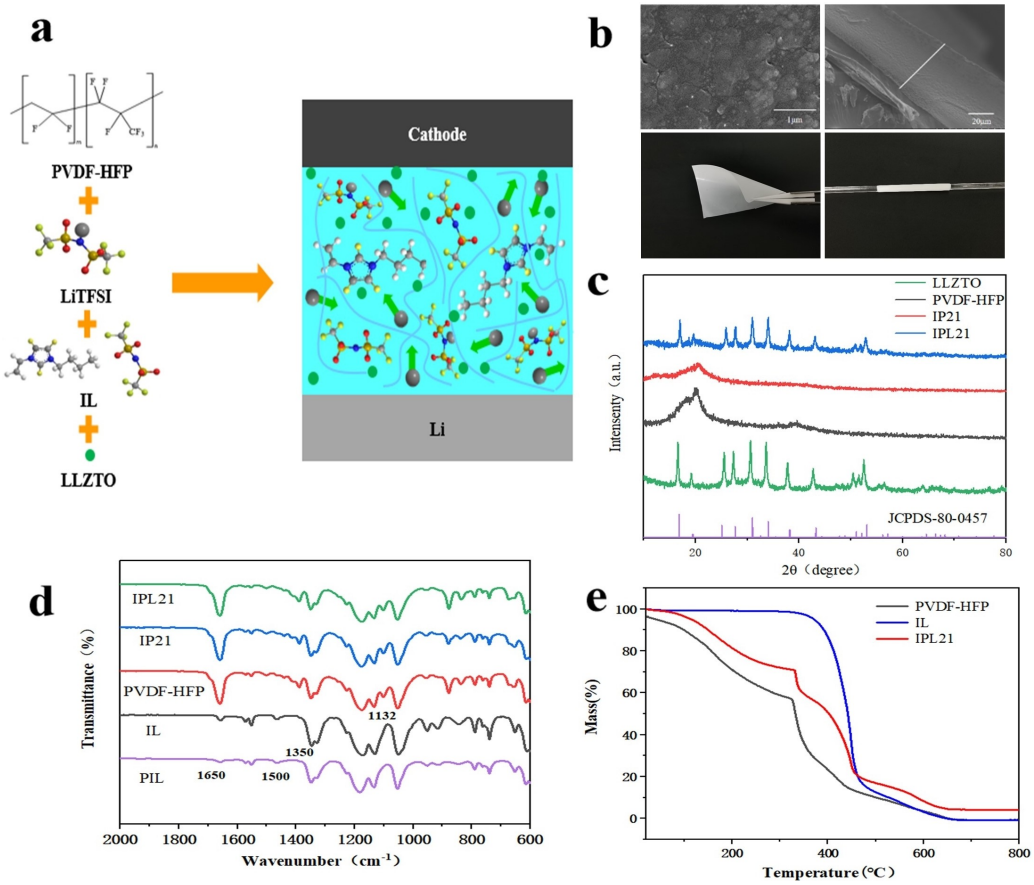

Figure 2. a) Schematic diagram of the IPL21-SPE. b) Digital photographs and microstructural SEM images of IPL21-SPE membrane, c) XRD patterns, d) FTIR spectra, e) TGA curves of IL, PH-SPE, IPL21-SPE.

liquid can inhibit the crystallization process and increase the amorphous region, which is more conducive to ion conduction. In addition, the cubic structure of LLZTO nanoparticles exhibits a well crystalline property.[26] After adding moderate LLZTO filler, the XRD peak related to PVDF-HFP becomes weaker and narrower, reflecting that LLZTO can effectively restrict the orderly arrangement of polymer chain and decrease the crystallinity. The reduction of crystallinity basically enhance the Li^+ conductivity of the IPL21-SPE film.[27] However, the Li^+ conductivity will be decreased with higher content of LLZTO nanoparticles, which impute to the high surface energy and aggregation.

The chemical structures of diverse electrolytes were measured by Fourier-transform infrared (FT-IR) spectroscopy. The FT-IR spectra of the IL, PIL and other polymer electrolytes of the experiment are shown in Figure 2(d). The typical peak located at 1650 cm^{-1} is attributed to the C=C stretching vibration of the IL. The decrease of peak value is due to the polymerization of part of IL formed PIL. The absorption peak is transferred to lower energy by addition of LLZTO fillers, indicating the interaction of LLZTO powder with the C=C of the IL polymer.[28] In the spectrum of IL, the peaks in 1350, 1170, 1130, and 1050 cm^{-1} are assigned to the S=O, CF_3, C–SO_2–N and S–N–S bonds of the imide anion ion $TFSI^-$, respectively.[29] No significant changes are observed, indicating a satisfied compatibility between PVDF-HFP and IL.

As shown in Figure 2(e), the thermal stability of IPL21-SPE was observed by thermogravimetric analysis (TGA). It is noteworthy that the IL remains stable over 300 °C without any decomposition phenomenon, which is superior to PH-SPE. The higher decomposition temperature indicates that a small quantity of PIL addition increase the safety property of the SPEs. The addition of LLZTO filler obviously enhanced the thermal stability of IPL21-SPE on account of the higher decomposition temperature of LLZTO than other electrolytes. This superior thermal stability assures safe operation in a broad temperature range.

In the course of battery charging and discharging, the transference of Li^+ will induce concentration polarization, which may have an important impact on the cycle performance of the cells. Consequently, high Li^+ transfer numbers (t_{Li+}) have a crucial impact on battery performance. The lithium ion transfer number of IPL21-SPE is 0.57 (Figure 3a), which is higher than that of PH-SPE (0.26), IP21-SPE (0.35) (Figure S5) and conventional liquid electrolyte (~0.2).[30] Polymerized ionic liquid crosslinking restricts the movement of large group ions, such as lithium salt anion ($TFSI^-$), hence IPL21-SPE has a higher number of ion migration. Moreover, it is relevant to the strong force between $TFSI^-$ and LLZTO ceramic filler. There are three

Research Article
doi.org/10.1002/batt.202300056
Chemistry Europe
European Chemical Societies Publishing

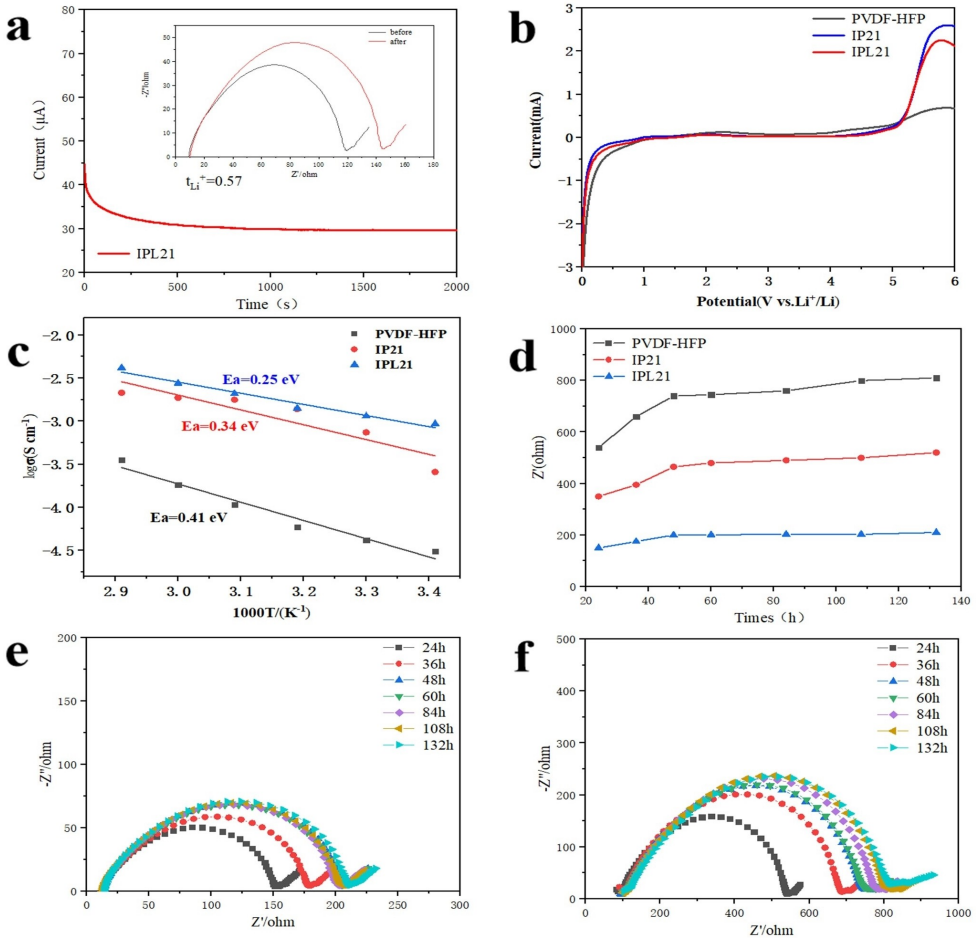

Figure 3. a) Direct current polarization curve for the IPL21-SPE, the EIS curves before and after polarization (the inset). b) LSV curves of PH-SPE, IP21-SPE and IPL21-SPE. c) Arrhenius plots of PH-SPE, IP21-SPE and IPL21-SPE. d) Curves of impedance value with time of PH-SPE, IP21-SPE and IPL21-SPE. e) Interfacial impedance response with time evolution of symmetrical Li/IPL21-SPE/Li cell at 25 °C. f) Interfacial impedance response with time evolution of symmetrical Li/IP21-SPE/Li cell at 25 °C.

reasons: 1) Partially dehydrofluorinated PVDF and the introduced LLZTO particles could complex with Li^+ via acid-base interaction, which can effectively dissociate lithium salt to increase Li^+ carrier density for conduction; 2) a highly conductive space charge layer is constituted between LLZTO fillers and polymer, which will decrease the activation energy of Li^+ transference; 3) There are a large number of vacancies on the ceramic surface, which contributes to Li^+ jump from vacancies to achieve transference.[31,32]

As depicted in Figure 3(b), the LSV measurement was implemented with a voltage ranging from 0 to 6 V at 25 °C. The results showed that PH-SPE began to decompose at about 4.0 V. When the ionic liquid polymer is added, the electrochemical window of IP21-SPE expands to about 5.0 V, which can totally satisfy the conditions of commercial lithium battery working voltage (4.2 V). With the further introduction of LLZTO fillers, the electrochemical window of IPL21-SPE was as high as 5.2 V. No electrochemical decomposition was discovered until 5.2 V, indicating that the IPL21-SPE membrane had superior tolerance of polarization and remained remarkable electrochemical stability for Li metal. As a result, the IPL21-SPE membrane could function well with high-voltage cathodes for high energy density batteries.[33]

By manifesting the relationship between the Li^+ conductivity and temperature, the Arrhenius curves of different SPEs were also demonstrated in Figure 3(c). The activation energy of IPL21-SPE is 0.25 eV, reflecting a lower Li^+ transfer energy barrier than IP21-SPE (0.34 eV) and PH-SPE (0.41 eV). The decrease of E_a indicates the lower energy barrier for Li^+ transport in IPL21-SPE than PH-SPE and IP21-SPE. Accordingly, the lower activation energy will benefit battery performance.[34] The Li^+ conductivity of PH-SPE and IP21-SPE films was about 3.11×10^{-5} S cm^{-1} and 2.67×10^{-4} S cm^{-1} at room temperature. The enhanced Li^+ conductivity of IP21-SPE was ascribed to the polymerization of ionic liquid. After a certain amount of LLZTO was added (Figures 3c and S4), the Li^+ conductivity of IPL21-SPE raised to 9.26×10^{-4} S cm^{-1}. The increase of Li^+ conductivity of IPL21-SPE may be due to the following reasons: 1) the polymerization of ionic liquid formed a three-dimensional cross-linked network, which was conducive to ion conduction; 2) the strong electronegativity of F atom in PVDF-HFP was conducive to ion transport; 3) the addition of LLZTO ceramic

Research Article
doi.org/10.1002/batt.202300056
Chemistry Europe
European Chemical Societies Publishing

filler further reduces the crystallinity of IPL21-SPE.[35–37] LLZTO could facilitate the dissociation of lithium salt through the strong force with anions, so as to enhance the concentration of dissociative lithium ion in the electrolyte. Therefore, the Li^+ conductivity of IPL21-SPE was higher than IP21-SPE. However, the excessive ceramic filler was disproportionately distributed in the polymer matrix, which reduces the influence of LLZTO on lithium salt and the obstruction of polymer chain.[38,39]

Figure 3(d) depicts the changes of the impedance values of the three electrolyte membranes with time. It is obvious that the changes of the impedance values tend to be stable with time, indicating excellent stability. Compared with the other two electrolyte membranes, IPL21-SPE has lower interface impedance, which is more conducive to the migration of Li^+ and the inhibition of lithium dendrite formation.

Figure 3(e, f) depicts the change of interface impedance of symmetric cell with time at room temperature. Figure S6(a) shows that the interface impedance of pure PH-SPE film continuously increases with extension of time and the maximum is about 515 Ω at 132 h. The interface resistance of IPL21-SPE membrane increases gradually with the extension of time. The interface resistance has a little change after 36 h and approaches the maximum about 210 Ω at 132 h, indicating that a stable SEI is formed on the lithium surface during this period. At the same time, the addition of PIL can build a viscoelastic interface between the electrode and the electrolyte, resulting in the reduction of interface impedance.[40]

The dynamic electrochemical stability of IPL21-SPE and electrodeposition of Li metal were investigated. Critical current density (CCD) is an important parameter to evaluate the capability of SPEs to suppress lithium dendrites.[41] The galvanostatic fitful cycling of the Li/IPL21-SPE/Li battery with amphitheatre increased current density was investigated to identify the critical current density. The voltage-time curves in the light of current density range from 0.05 to 0.85 mA cm^{-2} was shown in Figure 4(a). The polarization voltage almost linearly increases as expected with increasing current density, and no short circuit occurs when the current density is increased to 0.8 mA cm^{-2}. These results indicated that the interface between IPL21-SPE and Li metal revealed satisfied stability and compatibility as well as more effective to prevent lithium deposition. However, the polarization voltage increases sharply when the current density up to 0.85 mA cm^{-2}, indicating short circuit occurs.[34]

On the one hand, the constant current plating/stripping test was used to research the interface compatibility between metal lithium and electrolyte. On the other hand, we studied the effect of LLZTO and IL on the interface stability. As indicated in Figure 4(c), the polarization voltage of Li/IPL21-SPE/Li battery keep constant for 800 h at the current density of 0.1 mA cm^{-2}. The cycle lifespan of the symmetric battery has surpassed the consequence of multifarious SPEs reported in most literatures.[42,43] However, a prominent increase polarization occurred in Li/IP21-SPE/Li and severe short circuit occurred in Li/PH-SPE/Li battery after about 420 h and 220 h, respectively. These results exhibited that the addition of PIL and LLZTO realize stable deep circulation and small polarization. They play a crucial part in the amelioration of interface stability.

As shown in Figure 4(b), the voltage polarization remained stable over 200 h of constant Li stripping/plating. The response of the Li/IPL21-SPE/Li battery was satisfactory, indicating low

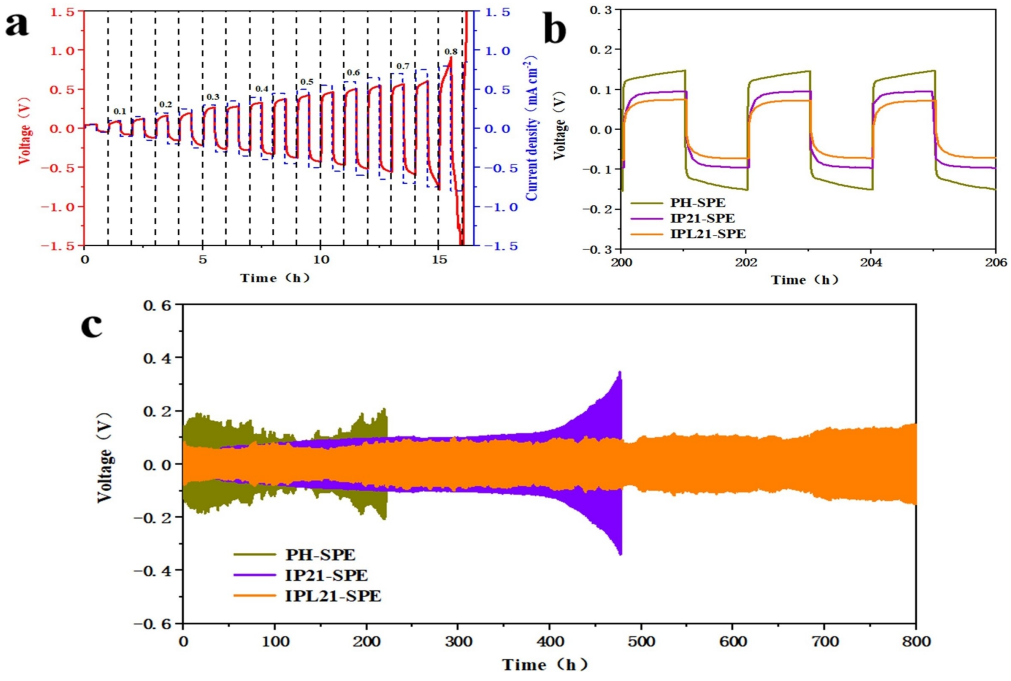

Figure 4. a) Galvanostatic intermittent cycling of the Li/IPL21-SPE/Li symmetric cells at step-increased current density at 50 °C. b) Magnified view of the Li plating/stripping performance of the symmetric cells. c) Plating/striping performances of symmetrical Li cells with PH-SPE, IP21-SPE, and IPL21-SPE at a current density of 0.1 mA cm^{-2}.

Research Article
doi.org/10.1002/batt.202300056
Chemistry Europe
European Chemical Societies Publishing

voltage polarization. Furthermore, the voltage distribution exhibited the stable interface between Li metal and IPL21-SPE. It will not result in local high current density and lithium dendrites in the edge area where the lithium metal contact with polymer electrolyte.[44,45] Meanwhile, Nyquist plots of Li/PH-SPE/Li, Li/IP21-SPE/Li and Li/IPL21-SPE/Li further explains the low interfacial resistance and excellent interface performance after plating/striping at a current density of 0.1 mA cm^{-2} (Figure S7).

For the purpose of proving the advantages of IPL21-SPE, a solid-state lithium metal battery was assembled with LFP cathode (1 C = 170 mA h g^{-1}), and the electrochemical properties were tested. The excellent electrochemical performance of IPL21-SPE can conduce to improve the rate property. The capacities of LFP/IPL21-SPE/Li cells are 162.1, 149.8, 124.1, and 102.1 mA h g^{-1} at 0.1, 0.2, 0.5, and 1.0 C, respectively (Figure 5a, b). When the current rates return to 0.2 C, the specific discharge capacity is renovated to 151.0 mA h g^{-1}, which indicates that the well reversibility and excellent rate cycle performance. On the contrary, the LFP/PH-SPE/Li cells have a lower discharge capacity at various current rates than that of LFP/IPL21-SPE/Li cells. In order to study the cycle stability of the LFP/IPL21-SPE/Li cells, an extra long-term cycle performance test was performed at a current rate of 0.5 C (Figure 5c). It is observed that a specific discharge capacity of 112.2 mA h g^{-1} and a high capacity retention rate of 94.1 % can be obtained over 100 cycles, which indicates the solid-state battery assembled with IPL21-SPE film have outstanding cycle stability.

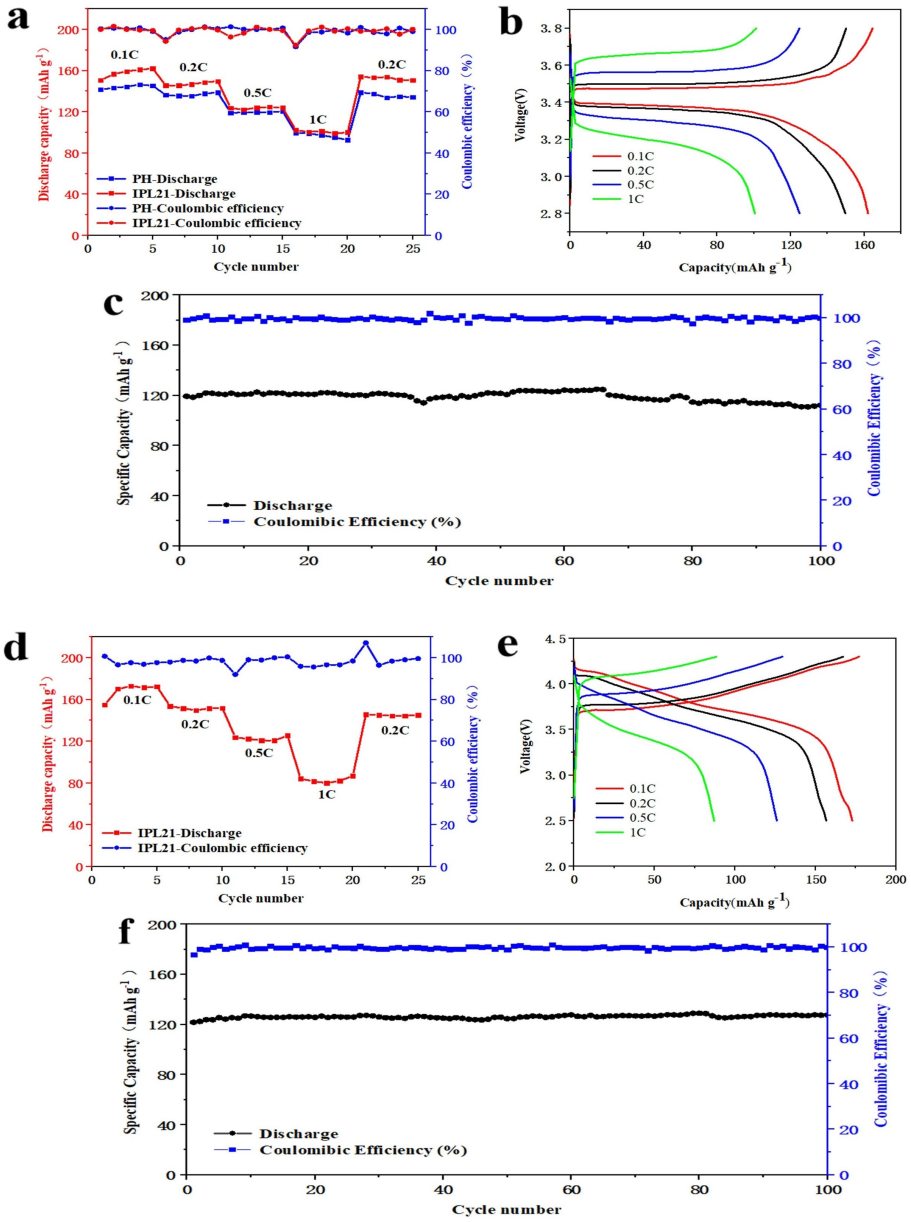

Figure 5. a) Rate performance of PH-SPE and IPL21-SPE at 25 °C. b) Charge-discharge profiles of the Li/IPL21-SPE/LFP cell at various rates. c) Cycling stability of 0.5 C at 25 °C, d) Rate performances of NCM811/Li SLMB assembled with IPL21-SPE. e) Charge-discharge profiles of the Li/IPL21-SPE/NCM811 cell at various rates and f) cycling stability of 0.5 C at 25 °C.

Research Article
doi.org/10.1002/batt.202300056
Chemistry Europe
European Chemical Societies Publishing

In addition, $LiNi_{0.8}Co_{0.1}Mn_{0.1}O_2$ (NCM811) (1 C = 200 mA h g^{-1}) was also selected as the high-voltage cathode to verify the availability of IPL21-SPE in the high energy-density batteries (Figure 5d, e). Within the operating testing voltage range of 2.5–4.3 V, the solid-state battery can provide a high specific discharge capacity of about 170 mA h g^{-1} at 0.1 C and 25 °C. Even though the current density increases to 0.5 C, the battery can output a high specific discharge capacity of 125 mA h g^{-1} and maintain a stable cycle with 100 cycles (Figure 5f). It proves the progress of IPL21-SPE matching with high voltage cathodes. This is mainly because the better high-pressure resistance inside the IPL21-SPE ensures that oxidative decomposition will not occur under high-pressure conditions. The specific discharge capacity of the NCM811/PH-SPE/Li cells is 97.8 mA h g^{-1} at a rate of 0.5 C, and shows poor cycling stability (Figures S8, S9). Compared with other polymer electrolytes, the IPL21-SPE membrane have better high-pressure resistance, well compatibility and stability with high-voltage cathode. Figure S10 displayed the resistance of NCM811/IPL21-SPE/Li before and after 100 cycles. The interfacial resistance decrease was attributed to the good compatibility between the electrolyte and the electrode.

In order to research the secure and flexible application of IPL21-SPE, a soft pack battery was assembled with it as shown in Figure 6. It could still glow at various fold angles without short-circuit. A portion of the remaining battery continues to light the LED device even after the battery was cut off. We measured the voltage of the battery before and after bending and cutting, the voltage was sufficient to light up the LED. There was not obviously changed in the brightness of LED because of the slight voltage change (Figure S11).[46,47] This indicates that the well tensile strength of electrolyte ensures that it still accomplish close cooperation between electrolyte and electrode in common cases, which has expansive application prospects.

Conclusions

In conclusion, a common and handy solution casting method has been exploited to fabricate IPL21-SPE. The results shows that polymerized ionic liquid and nano filler LLZTO can effectively improve the interface compatibility, room temperature ionic conductivity (9.26×10^{-4} S cm^{-1}) and lithium ion transfer number (0.57). The SPEs shows a broad electrochemical window as high as 5.2 V. Furthermore, the uniform lithium deposition has been induced because of the multiple fast Li^+ transport pathways in SPEs that can effectually adjust Li^+ flux. Therefore, the stable interface layer ensures the Li symmetrical battery equably plating/stripping over 800 h. What's more, the electrolyte equipped with $LiFePO_4$ and NCM811 cathodes both exhibit prominent battery performances in SLMBs. The $LiFePO_4$/IPL21-SPE/Li cells retain a high-capacity retention ratio over 94.1 % at 0.5 C after 100 cycles. In terms of practical applications, the assembled $LiFePO_4$/Li pouch cell give evidence of responsible safety and applied flexibility. The design of solid polymer electrolyte based on polymerized ionic liquid provides a promising method for high-performance solid-state lithium metal battery, and is expected to realize commercial application of SLMBs.

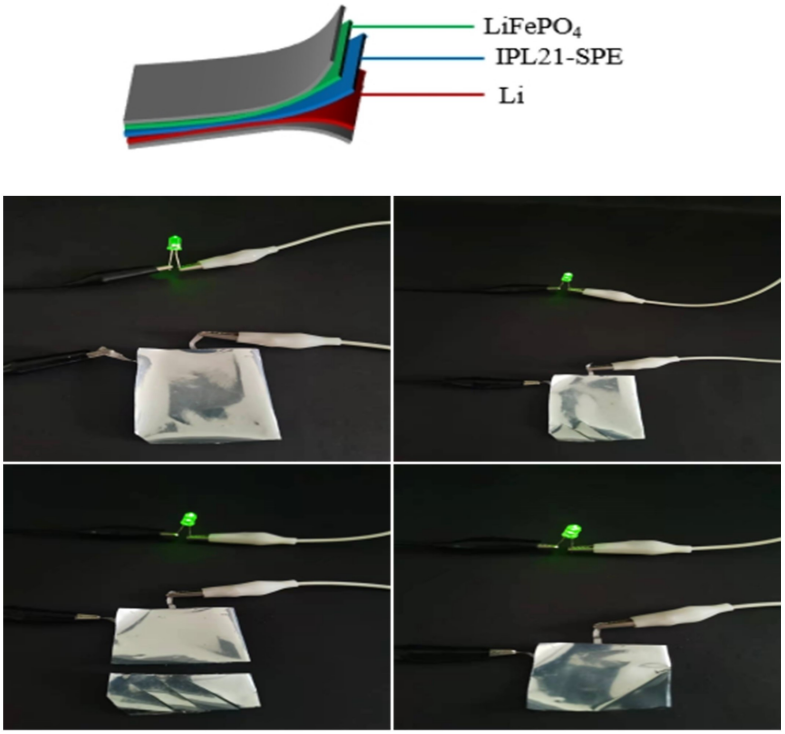

Figure 6. Schematic diagram of the structure of the $LiFePO_4$/IPL21-SPE/Li pouch cell and the performance test for lighting the LED at both bending and shearing conditions.

Research Article
doi.org/10.1002/batt.202300056
Chemistry Europe
European Chemical Societies Publishing

Experiments Section

Materials

1-butyl-3-vinylimidazolium bis((trifluoromethyl) sulfonyl)imide (VBImNTF2) was provided by Lanzhou Institute of Chemical Physics. 2,2′-Azobis(2-methylpropionitrile) (AIBN), bis(trifluoromethane)sulfonimide lithium salt (LiTFSI) were used as received from Aladdin. N,N-dimethylformamide (DMF) was purchased from Tianjin Guangcheng Chemical Reagent Co. Ltd. Lithium iron phosphate ($LiFePO_4$), acetylene black and poly(vinylidene fluoride) (PVDF) were acquired by Lizhiyuan Battery Materials Co. Ltd. $Li_{6.4}La_3Zr_{1.4}Ta_{0.6}O_{12}$ (LLZTO) was purchases form Hefei Kejing materials technology Co. Ltd and Poly(vinylidene fluoride-co-hexa-fluoropropylene) (PVDF-HFP, average Mw ~ 400000) was provided by Aladdin.

Preparation of SPE films

The solid polymer electrolyte films were prepared by the solution casting method. Firstly, the PVDF-HFP and LiTFSI were added into N,N-Dimethylformamide and stirred for 2 h at 60 °C to acquire a uniformly dispersed solution, and the proportion of IL/PVDF-HFP was 2 : 1 (marked as IP21) and AIBN were added into the solution. SPE films (marked as IPL21) were obtained by adding 10 % of LLZTO powder (mass ratio) and stirred for 8 h. Subsequently, the well uniformly dispersed solution was poured into the Teflon mold and vacuum-dried at 60 °C for 24 h.

Structure characterization and electrochemical measurements

The X-ray diffraction (XRD) patterns investigated the crystallinity degree of diverse electrolytes. The surface morphology of IPL21-SPE was observed by SEM (Hitachi Regulus 8220). FT-IR analysis was performed for the molecular structure. TGA was conducted with a NETZSCH STA 449F5 analyzer under an argon atmosphere with a heating rate of 5 °C min^{-1}. The tensile property was performed by WDW-02 with a stress rate of 10 mm min^{-1}.

The ion conductivity (σ) was analyzed by electrochemical impedance spectroscopy (EIS) in the frequency range from $10^{-1} \sim 10^5$ Hz. Then σ was calculated according to the equation:

$$\sigma = \frac{L}{RS} \tag{1}$$

where L (cm) is the thickness of the IPL21-SPE, S (cm^{-2}) belongs to the contacting area of the stainless steel (SS), while R is the bulk resistance. The Li-ion transfer number (t_{Li+}) was explored via Li/Li symmetric cell, and the calculation equation as follows:

$$t_{Li}^{+} = \frac{I_{ss}(\Delta V - I_0 R_0)}{I_0(\Delta V - I_{ss} R_{ss})} \tag{2}$$

where the potential amplitude ΔV is 10 mV, I_0 and I_{SS} are the initial and steady-state current of the cell in DC polarization. R_0 and R_{SS} represent the initial and steady-state interface resistance obtained from the AC impedance test. The sandwich cell of SS/SPE/Li was used for the test of electrochemical window via linear sweep voltammetry (LSV) in a potential range of 0 to 6 V. In addition, the assembled Li//LFP cells were conducted in a potential range of 2.8–3.8 V (1 C = 170 mA h g^{-1} for LFP) via LAND testing system to obtain the electrochemical performance.

Acknowledgments

The authors gratefully acknowledge the financial support from National Natural Science Foundation of China (21908233) and the Introduction and Cultivation Plan of Young Innovative Talents in Colleges and Universities of Shandong Province.

Conflict of Interests

The authors declare no conflict of interest.

Data Availability Statement

The data that support the findings of this study are available from the corresponding author upon reasonable request.

Keywords: in-situ polymerization · ionic conductivity · ionic liquid · $Li_{6.4}La_3Zr_{1.4}Ta_{0.6}O_{12}$ · LLZTO · solid polymer electrolytes

[1] S. Xin, Y. You, S. Wang, H.-C. Gao, Y.-X. Yin, Y.-G. Guo, *ACS Energy Lett.* **2017**, *2(6)*, 1385–1394.
[2] W. L. Huang, N. Zhao, Z. J. Bi, C. Shi, X. X. Guo, L. Z. Fan, C. W. Nan, *Materials Today Nano* **2020**, *10*, 100075.
[3] T. Famprikis, P. Canepa, J. A. Dawson, M. S. Islam, C. Masquelier, *Nat. Mater.* **2019**, *18*, 1278–1291.
[4] R. Chen, Q. Li, X. Yu, L. Chen, H. Li, *Chem. Rev.* **2020**, *120*, 6820.
[5] X. Yang, K. R. Adair, X. Gao, X. Sun, *Energy Environ. Sci.* **2021**, *14*, 643–671.
[6] M. H. Ge, X. Y. Zhou, Y. P. Qin, Y. Liu, J. J. Zhou, X. L. Wang, B. K. Guo, *Chin. Chem. Lett.* **2022**, *33*, 3894–3898.
[7] A. Banerjee, X. Wang, C. Fang, E. A. Wu, Y. S. Meng, *Chem. Rev.* **2020**, *120*, 6878.
[8] J. Dai, C. Yang, C. Wang, G. Pastel, L. Hu, *Adv. Mater.* **2018**, *30*, 1802068.
[9] Z. Bi, S. Mu, N. Zhao, W. Sun, W. Huang, X. Guo, *Energy Storage Mater.* **2021**, *35*, 512–519.
[10] D. Zhang, X. Xu, Y. Qin, S. Ji, Y. Huo, Z. Wang, Z. Liu, J. Shen, J. Liu, *Chem. Eur. J.* **2020**, *26*, 1720–1736.
[11] X. Yang, M. Jiang, X. Gao, D. Bao, Q. Sun, N. Holmes, H. Duan, S. Mukherjee, K. Adair, C. Zhao, J. Liang, W. Li, J. Li, Y. Liu, H. Huang, L. Zhang, S. Lu, Q. Lu, R. Li, C. V. Singh, X. Sun, *Energy Environ. Sci.* **2020**, *13*, 1318–1325.
[12] B. Tong, Z. Y. Song, H. Wu, X. X. Wang, W. F. Feng, Z. B. Zhou, H. Zhang, *Mater. Futures.* **2022**, *1(4)*, 042103.
[13] K. Pan, L. Zhang, W. Qian, X. Wu, K. Dong, H. Zhang, S. Zhang, *Adv. Mater.* **2020**, *32*, 2000399.
[14] M. Yao, A. Liu, C. Xing, B. Li, S. Pan, J. Zhang, P. Su, H. Zhang, *Chem. Eng. J.* **2020**, *394*, 124883.
[15] Z. Wan, D. Lei, W. Yang, C. Liu, K. Shi, X. Hao, L. Shen, W. Lv, B. Li, Q.-H. Yang, F. Kang, Y.-B. He, *Adv. Funct. Mater.* **2019**, *29*, 1805301.
[16] Y. Cheng, J. Shu, L. Xu, Y. Xia, L. Du, G. Zhang, L. Mai, *Adv. Energy Mater.* **2021**, *11*, 2100026.
[17] W. Zhou, Z. Wang, Y. Pu, Y. Li, S. Xin, X. Li, J. Chen, J. B. Goodenough, *Adv. Mater.* **2019**, *31*, 1805574.
[18] P. N. Didwal, Y. N. Singhbabu, R. Verma, B.-J. Sung, G.-H. Lee, J.-S. Lee, D. R. Chang, C.-J. Park, *Energy Storage Mater.* **2021**, *37*, 476–490.
[19] A. R. Polu, H.-W. Rhee, *Int. J. Hydrogen Energy* **2017**, *42*, 7212–7219.
[20] Y. S. Ye, J. Rick, B. J. Hwang, *J. Mater. Chem. A* **2013**, *1*, 2719–2743.
[21] S. Y. Lang, Y. Shi, Y. G. Guo, D. Wang, R. Wen, L. J. Wan, *Angew. Chem.* **2016**, *128*, 16067–16071.
[22] Q. Ma, X. X. Zeng, J. Yue, Y. X. Yin, T. T. Zuo, J. Y. Liang, Q. Deng, X. W. Wu, Y. G. Guo, *Adv. Energy Mater.* **2019**, *9*, 1803854.
[23] F. L. Xu, S. G. Deng, Q. Y. Guo, D. Zhou, X. Y. Yao, *Small Methods* **2021**, *5*, 2100262.
[24] Y. G. Cho, C. Hwang, D. S. Cheong, Y. S. Kim, H. K. Song, *Adv. Mater.* **2018**, *31*, 1804909.

[25] C. Z. Zhao, P. Y. Chen, R. Zhang, X. Chen, B. Q. Li, X. Q. Zhang, X. B. Cheng, Q. Zhang, *Sci. Adv.* **2018**, *4*, eaat3446.
[26] R. J. Chen, Y. B. Zhang, T. Liu, B. Q. Xu, Y. H. Lin, C. W. Nan, Y. Shen, *ACS Appl. Mater. Interfaces* **2017**, *9*, 9654–9661.
[27] Y.-C. Lin, J.-H. Cheng, V. M, F.-M. Wang, R. Santhanam, B. J. Hwang, *J. Chin. Chem. Soc.* **2012**, *59*, 1250–1257.
[28] T. A. Zegeye, W.-N. Su, F. W. Fenta, T. S. Zeleke, S.-K. Jiang, B. J. Hwang, *ACS Appl. Energ. Mater.* **2020**, *3*, 11713–11723.
[29] D. Zhang, Z. Liu, Y. Wu, S. Ji, Z. Yuan, J. Liu, M. Zhu, *Adv. Sci.* **2022**, *9*, 2104277.
[30] C. Z. Zhao, X. Q. Zhang, X. B. Cheng, R. Zhang, R. Xu, P. Y. Chen, H. J. Peng, J. Q. Huang, Q. Zhang, *Proc. Natl. Acad. Sci. USA* **2017**, *114*, 11069–11074.
[31] X. Wang, X. Hao, Z. Hengjing, X. Xia, J. Tu, *Electrochim. Acta* **2020**, *329*, 135108.
[32] J. Zhang, X. Zang, H. Wen, T. Dong, J. Chai, Y. Li, B. Chen, J. Zhao, S. Dong, J. Ma, L. Yue, Z. Liu, X. Guo, G. Cui, L. Chen, *J. Mater. Chem.* **2017**, *5*, 4940–4948.
[33] Y. Li, W. Zhang, Q. Dou, K. W. Wong, K. M. Ng, *J. Mater. Chem. A* **2019**, *7*, 3391–3398.
[34] Z. Y. Wang, L. Shen, S. G. Deng, P. Cui, X. Y. Yao, *Adv. Mater.* **2021**, *33*, 2100353.
[35] C. Fu, G. Homann, R. Grissa, D. Rentsch, W. Zhao, T. Gouveia, A. Falgayrat, R. Lin, S. Fantini, C. Battaglia, *Adv. Energy Mater.* **2022**, *12*, 2200412.
[36] J. Huang, Y. Huang, Z. Zhang, H. Gao, C. Li, *Energy Fuels* **2020**, *34*, 15011–15018.
[37] X. Wang, G. M. A. Girard, H. Zhu, R. Yunis, D. R. MacFarlane, D. Mecerreyes, A. J. Bhattacharyya, P. C. Howlett, M. Forsyth, *ACS Appl. Energ. Mater.* **2019**, *2*, 6237–6245.
[38] Z. Xue, D. He, X. Xie, *J. Mater. Chem. A* **2015**, *3*, 19218–19253.
[39] T.-C. Wang, C.-Y. Tsai, Y.-L. Liu, *ACS Sustainable Chem. Eng.* **2021** *9*, 6274–6283.
[40] J. L. Schaefer, S. S. Moganty, D. A. Yanga, L. A. Archer, *J. Mater. Chem.* **2011**, *21*, 10094–10101.
[41] Y. Su, X. D. Zhang, C. C. Du, Y. Luo, J. Z. Chen, J. T. Yan, D. D. Zhu, L. Geng, S. X. Liu, J. Zhao, Y. S. Li, Z. Y. Rong, Q. Huang, L. Q. Zhang, Y. F. Tang, J. Y. Huang, *Small* **2022**, *18*, 2202069.
[42] D. Zhou, D. Shanmukaraj, A. Tkacheva, M. Armand, G. Wang, *Angew. Chem.* **2019**, *5*, 2326–2352.
[43] Q. Zhao, X. Liu, S. Stalin, K. Khan, L. A. Archer, *Nat. Energy* **2019**, *4*, 365–373.
[44] S. A. Pervez, G. Kim, B. P. Vinayan, M. A. Cambaz, M. Kuenzel, M. Hekmatfar, M. Fichtner, S. Passerini, *Small* **2020**, *16*, 2000279.
[45] P. Chen, X. Liu, S. Wang, Q. Zeng, Z. Wang, Z. Li, L. Zhang, *ACS Appl. Mater. Interfaces* **2019**, *11*, 43146–43155.
[46] T.-Q. Yang, C. Wang, W.-K. Zhang, Y. Xia, Y.-P. Gan, H. Huang, X.-P. He, J. Zhang, *Rare Met.* **2022**, *41(6)*, 1870–1879.
[47] Q. Y. Guo, F. L. Xu, L. Shen, S. G. Deng, Z. Y. Wang, M. Q. Li, X. Y. Yao, *Energy Mater. Adv.* **2022**, *Article ID: 9753506*.

Manuscript received: February 17, 2023
Revised manuscript received: April 10, 2023
Accepted manuscript online: April 10, 2023
Version of record online: April 27, 2023